Statistical Measures of Planck Scale Signal Correlations in Interferometers

Craig J. Hogan

University of Chicago and Fermilab Center for Particle Astrophysics

Ohkyung Kwon[a]

University of Chicago and Korea Advanced Institute of Science and Technology

A model-independent statistical framework is presented to interpret data from systems where the mean time derivative of positional cross correlation between world lines, a measure of spreading in a quantum geometrical wave function, is measured with a precision smaller than the Planck time. The framework provides a general way to constrain possible departures from perfect independence of classical world lines, associated with Planck scale bounds on positional information. A parameterized candidate set of possible correlation functions is shown to be consistent with the known causal structure of the classical geometry measured by an apparatus, and the holographic scaling of information suggested by gravity. Frequency-domain power spectra are derived that can be compared with interferometer data. Simple projections of sensitivity for realistic experimental set-ups suggests that measurements will confirm or rule out a class of Planck scale departures from classical geometry.

I. INTRODUCTION

Although it is widely believed that the world follows quantum principles, it is not known how classical dynamical space-time emerges from a quantum mechanical system [1–3]. Standard field theory, often regarded as the basis of a fundamental quantum theory, encounters well-known, unavoidable divergences at the Planck scale [4–6]. The divergences may be avoided in a theory based on other fundamental objects such as strings[7–9], loops or spin networks[1–3], and/or noncommutative geometries[10]; these theories can even lead to predictions of new behavior at the Planck scale, such as quantization of volume or area. However, for large systems, many issues remain unresolved, for example, the foundational inconsistency of quantum theory with the "local realism" associated with classical geometrical paths and events[11–14], the holographic encoding of information in dynamical gravitational systems, particularly black holes[15–24], and unphysically large masses of some field systems in large volumes[25, 26].

Most theoretical attention has concentrated on the ultraviolet part of the problem— the Planck scale regime dominated by string theory. On the other hand, the large-scale or infrared paradoxes also presumably arise because field theory is quantized on a fixed classical background, whereas the real space-time system emerges, along with the classical notion of locality, from a quantum system based on a Planckian bandwidth limit or discrete structure. While ultraviolet effects at the Planck scale cannot be measured directly, scaling from standard quantum mechanics suggests that indirect effects of Planck scale physics may be detectable in certain kinds of measurements in laboratory systems via spreading of geometrical position states over macroscopic distance. These arguments are reviewed below in section II A.

Correlations signifying departures from perfect classical space could plausibly appear, according to standard quantum mechanics, on a scale given by diffraction of Planck frequency radiation propagating across an apparatus, or equivalently, the quantum position uncertainty of a Planck mass particle over a duration corresponding to an apparatus light-crossing time [26–30]. Field theory assumes a classically coherent background geometry, and predicts that such nonlocal quantum correlations of the background should be negligible.

Although the approximate magnitude of the correlations can be guessed from scaling, their detailed character is not known. In the absence of a standard theory for large systems in emergent geometry, in this paper we take an empirical, experimental approach to the problem. We ask, what can precise laboratory measurements of the relative positions of massive bodies at rest tell us about the character of positional information contained in the space-time itself, and in particular, the detailed degrees of freedom of the quantum system that gives rise to space and locality? We focus on what can be learned about the emergence of classical positions in space from the best available technique for nonlocal measurement of position, interferometry[31].

The predictions of any quantum theory are expressed in terms of correlations between observables. In the case of a space-time built from a quantum system, departures from classicality should appear in time-averaged correlations of positions of massive bodies. For a given configuration of massive bodies— for example, the mirrors in an interferometer— the forms that the correlation functions can take are constrained by general principles of symmetry

[a] E-mail: o.kwon@kaist.ac.kr

and causality of the emerged space. We argue here that possible forms can be classified and evaluated from the known structure of a macroscopic apparatus, without knowing the elements and dynamics of the underlying quantum space-time degrees of freedom.

As one example of an observable correlation, signals from a pair of interferometers can be combined into a correlation function, whose mean time derivative has the dimension of time. If that has a value of the order of the Planck time, the information content of the measured spatial relationships is comparable with the total information content suggested by covariant holographic bounds on entropy [27–30, 32]. Interferometers are now capable of achieving measurements of coherence with Planck precision[33–38], so the framework presented here can be used to interpret their signals in terms of Planck scale bounds on information.

The goal is to use data to test a general hypothesis: that geometrical information about directions between world lines in space, defined by measurements of the position of massive bodies with electromagnetic waves, obeys Planck scale covariant constraints on information. With the framework presented here, statistical properties of data in a broad class of experiments can be compared with each other, and used to test specific forms of this general hypothesis, even in the absence of a specific fundamental theory. Experiments can explore and constrain any form of Planckian correlations in space-time position consistent with symmetries imposed by the causal structure of the emergent system.

We apply our framework here to a particular kind of apparatus, a correlated pair of Michelson interferometers, such as the Fermilab Holometer[35, 36], and also discuss how it can be generalized. In previous work[27–30, 32], specific models of holographic spatial position states were used to predict properties of measurable "holographic noise" in interferometers. The more general framework here allows a broader class of quantum models to be tested, even some with no corresponding classical interpretation. In all cases, the coherence is characterized by a key universal parameter: the time derivative of a measured correlation function, normalized to the size of an apparatus. We propose a scheme that spans the full range of possible models, characterized by two universal parameters of the order of the Planck time that can be directly constrained by data.

Of course, different experimental set-ups, with different causal relationships between the world lines of their optical elements, will constrain Planckian departures from classical coherence in different ways. We do not exhaust all those possibilities here, but general principles of this framework can be extended to compare them with each other and with predictions of proposed theories. For example, the Michelson systems mainly considered here (and used in the initial stage of the Holometer) measure only correlations spatially related by shear or strain transformations; they do not measure the important independent modes corresponding to pure rotations[39, 40]. Those modes, and apparatus that could measure them in a future experimental program at the Holometer, will be treated in upcoming analyses.

II.   GENERAL FRAMEWORK

A.   Scaling of Geometrical Correlations

Causal diamonds are defined as the 4-volume of spacetime over which an observer (defined by a timelike world-line) can do experiments. It is bounded by two null light-cones connecting two points on the observer's world-line that are timelike separated (see Figure 1). A world line defines a causal diamond associated with any proper time interval of duration τ. It has been proposed that nested sequences of causal diamonds— covering increasing intervals along a timelike trajectory— correspond to sequences of nested Hilbert spaces [13, 14]. These causal diamonds serve as reference boundaries for geometrical information.

Consider an observable operator $\hat{x}$, with the dimension of length, that characterizes a set of world lines in some extended 4D volume of flat space-time. In general, a measurement of $\hat{x}$ requires nonlocal propagation of light within a causal diamond; it represents a projection of an extended 4D quantum system. In the interferometer systems considered here, an observable signal depends on the world lines of an arrangement of mirrors, and encodes nonlocal information about their positions and about the state of the laser field. Here, we ignore these standard quantum degrees of freedom; the operators $\hat{x}$ measure new noncommuting degrees of freedom that differ from the standard motion[41] of a massive body in a classical geometry. A measurement of $\hat{x}$ represents a measurement of positional degrees of freedom that are assumed to be classical in the standard quantization of fields and optical elements in an interferometer[42, 43]. They correspond to new degrees of freedom associated with the nonclassical character of emergent world lines; thus, we know neither the Hamiltonian nor the conjugate operators for $\hat{x}$. (Other forms of entanglement with Planck scale geometrical states have been discussed in ref. [44].)
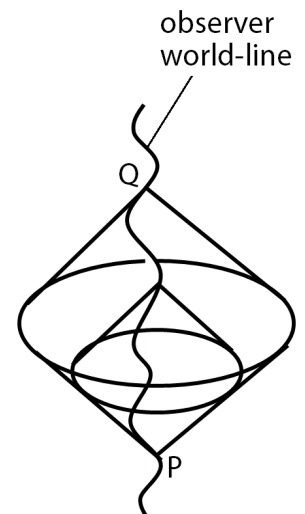

FIG. 1. Causal diamonds.

The value of $\hat{x}$ does not depend on the masses or other properties of bodies, only on their relative positions.

Suppose that the measured value of $\hat{x}$ departs by some amount $\Delta x = \hat{x} - \bar{x}$ from its expected value $\bar{x}$ in classical space-time. A measure of the deviation from perfect classical coherence is given by a time-domain correlation function of the form,

$$\Xi(\tau) \equiv \langle \Delta x(t) \Delta x(t+\tau) \rangle_t F(\tau). \tag{1}$$

Here, $F(\tau)$ denotes a projection determined by the configuration of a measurement apparatus. In general, correlations can be measured for two world lines, say $\hat{x}_A$ and $\hat{x}_B$; most of this paper focuses on the configurations where A and B causal diamonds are almost the same.

The positional correlation encoded in Ξ measures a lack of independence of values of $\hat{x}$. In a classical space-time, Ξ vanishes; this is possible because the information density in a continuum is infinite. The same is true in field theory, which assumes a classical continuous space-time. In an emergent quantum space-time, Ξ in general does not vanish, and the positions of world-lines in some measurements can decohere gradually with time. The 2D density of position eigenstates— that is, the number of independent world-line eigenstates per 2-volume in a particular $\hat{x}$ projection— has a finite value given by Ξ^{-1}. Its value depends on the projection defined by the measurement, and the invariant classical positional relationships between the world lines, particularly the causal diamonds traced by light propagation in the apparatus.

The scaling with τ can be estimated from dimensional considerations, or from analogy with other, standard quantum systems. It is plausible that world lines decohere slightly at long durations, by an amount that would not yet have been detected. As one example of a quantum system with this behavior, consider the standard position wave function for the state of a particle of mass m at rest, that lasts for duration τ. This form of standard Heisenberg uncertainty can be derived in several ways[26–29], for example from a nonrelativistic Schrödinger equation for a mass m, in a path integral approach by extremizing the action of a particle or body whose motion is described by a wave equation with de Broglie wavelength $\hbar/mc$, or from a Wheeler-De Witt equation for a pendulum of mass m in the low frequency, nearly free particle limit. For all of these systems, with the standard assumption that directions in space are independent, the wave function in classical position and time obeys

$$(\partial_i \partial^i - 2i(m/\hbar)\partial_t)\psi = 0. \tag{2}$$

This equation can be solved with pure (infinite) plane wave eigenmodes. However, the state of a body localized in space, whose position is prepared and measured at two times separated by an interval much longer than the inverse de Broglie frequency, is better described by a symmetric gaussian solution for $\psi(r,t)$, where $r^2 = x_i x^i$, with a probability density on constant-time surfaces given by

$$|\langle \psi^* | \psi \rangle|^2 \propto e^{-r^2/\sigma(t)^2}, \tag{3}$$

whose variance σ^2 depends on the preparation of the state.

These "paraxial" solutions for matter de Broglie waves are mathematically the same as the standard normal modes of light[45] in a laser cavity (see Figure 2). In the matter system, t takes the place of the laser beam axis coordinate z (that is, constant-phase de Broglie wavefronts are nearly surfaces of constant time), and position measurements at particular times, over an interval much smaller than the interval between measurements, takes the place of thin mirror surface boundary conditions [26]. In this family of solutions, the rate of spatial spreading depends on the preparation of a state: $d\sigma/dt$ is smaller for larger σ. In the same way that a larger beam waist leads to a smaller dispersion angle, a larger position uncertainty leads to slower spreading. Spreading of the wave function with time is unavoidable; any solution of duration τ has a mean variance of position at least as large as

$$\langle (r(t+\tau) - r(t))^2 \rangle = \sigma_0^2(\tau) > \hbar\tau/2m. \tag{4}$$

Thus, $d\sigma_0/d\tau = \hbar/2m$ gives the minimum rate of spreading in the position state of a body at rest over time.

Of course, these states also have an associated indeterminacy of momentum. Although the particle is classically "at rest", and there is a well defined expectation value for its rest frame, the actual velocity is indeterminate. In this situation, the position variance between two times cannot be "squeezed away" into momentum uncertainty, or vice versa; Eq. (4) gives the minimum spread of position between two times for *any* state [42, 43, 46]. The momentum uncertainty in the minimum-position-uncertainty state decreases with τ like $\Delta p \approx (2m\hbar/\tau)^{1/2}$, which is why de Broglie wave states behave almost like classical world lines on large scales.

Similarly, if paths in a background quantum space time are described by quantum wave propagation similar to Eq. (2), with a fundamental timescale set by the Planck time (that is, setting $m = m_P = \hbar/c^2 t_P$), then its emergent world line states spread over duration τ by about

$$\Xi(\tau) \approx \langle (x(t+\tau) - x(t))^2 \rangle \approx c^2 \tau t_P/2. \tag{5}$$
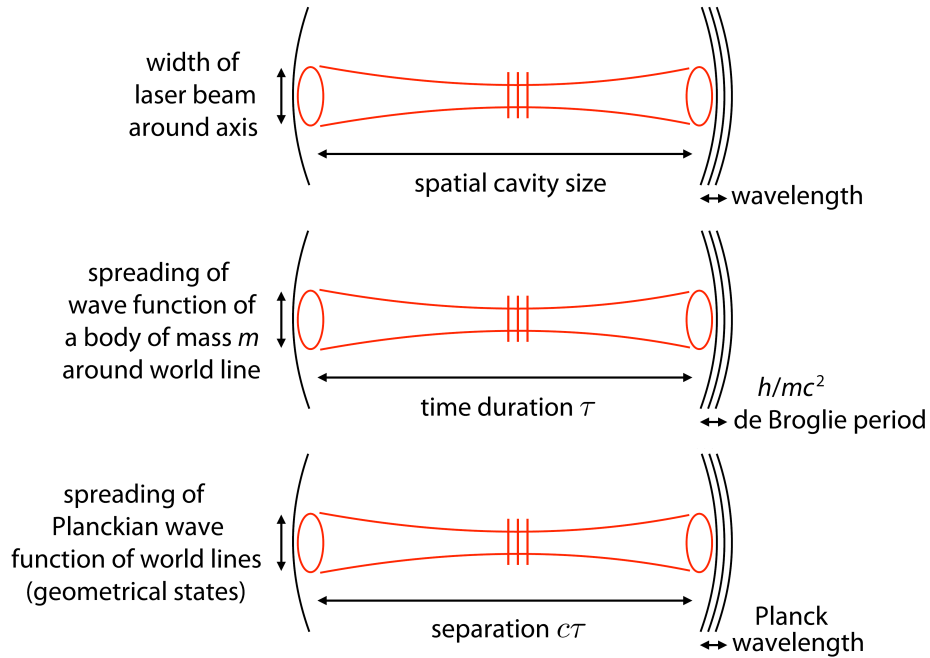
FIG. 2. Paraxial solutions and "world tubes."

To be sure, this background spreading cannot be detected by a local measurement, in the same way that quantum decoherence between independent paths of mass m_P bodies can be measured by comparing their positions, because the geometrical states of nearby world lines are entangled with each other. It may also include exotic correlations between different directions and components of position, which we have not included. However, the scaling of $\sigma_0^2(\tau)$ and $\Xi(\tau)$ with τ are the same: world lines should decohere at a rate given approximately by $d\Xi/d\tau \approx c^2 t_P/2$.

Figure 2 shows the mathematical parallels. The spreading of the wave function of a body of mass m around its world line over a duration τ (which we can loosely think of as "world tubes") is seen as mathematically similar to the spreading of a Planckian wave function describing emergent world line states over a separation $c\tau$, once the fundamental scale is set via the Planck mass. These "world tubes" can now describe the decoherence of geometrical states.

For large systems (that is, $\tau \gg t_P$), the variance of position is much larger than the typical value $\Xi \approx c^2 t_P^2$ from Planck scale field fluctuations on a classical background. At the same time, the variance is very small, and the trajectories behave nearly classically. Because the deviation can only be seen in a highly precise nonlocal measurement of correlations, it would not have been detected in previous experiments. A 100m laboratory scale experiment is $\approx 10^{37}$ Planck lengths across; Planckian spreading on the corresponding timescale ($10^{37} t_P \approx 10^{-6}$ sec) is only $\approx 10^{18.5} c t_P \approx 10^{-16.5}$ meters, and the typical variation in rest frame velocity is about $\approx 10^{-18.5} c$, or a few mm per year— an order of magnitude slower than continental drift.

The same scaling is suggested by applying holographic bounds to information in the relative position of world lines. The holographic principle posits covariantly that the information $\mathcal{I}$ in a causal diamond of duration τ is one quarter of the area of its bounding surface in Planck units, or $\mathcal{I}_H = (\pi/4)(\tau/t_P)^2$ in flat space. Suppose that the position operator $\hat{x}$ depends on positions distributed over a 3-volume $\approx (c\tau)^3$, and that the density of information in the radial dimension of the causal diamond has some value ℓ_r^{-1} in its rest frame, independent of system size. The number of position states is then $\mathcal{I}_x \approx (c\tau)^3 \ell_r^{-1} \Xi^{-1}$. If we require that $\mathcal{I}_x < \mathcal{I}_H$, so that the holographic information bound applies to spatial information, we obtain

$$\Xi(\tau) > \tau(c^3 t_P^2/\ell_r)(\pi/4). \tag{6}$$

Thus, there is some universal value of $\dot{\Xi} \equiv d\Xi/d\tau$ associated with holographic scaling of position information. Since the natural value of ℓ_r is of order ct_P, the natural value for $\dot{\Xi}$ is again of order $c^2 t_P$.

The value of $\dot{\Xi}$ depends on the configuration of the world lines represented in the operator $\hat{x}$. For some $\hat{x}$ operators that do not measure degrees of freedom where the information is bounded, it may vanish by symmetry; that is, the uncertainty could be squeezed into unmeasured degrees of freedom. Although the analogy (Eq. 2) is suggestive of how solutions should scale, we do not know how measurements in different directions, or between different world lines,

should relate to each other, or how the wave function should be interpreted physically. The experimental program is to measure correlations where we can, and perhaps uncover clues to the underlying theory.

The current exercise is to lay out statistical measures that can measure the value of $\dot{\Xi}$ with data from simple experimental setups. The form of Ξ can be constrained from general considerations about the causal diamonds corresponding to the arrangement of mirrors in an apparatus, so well-characterized universal conclusions about quantum geometry can be drawn from a specific experimental result.

B. Constraints on Correlations in Interferometer Signals

Consider two Michelson interferometers, A and B, with dark port signals $x_A(t)$ and $x_B(t)$ calibrated in length units. The statistical quantity estimated from a time stream of data is a cross-correlation between interferometers A and B:

$$\Xi(\tau) \equiv \langle x_A(t)x_B(t+\tau)\rangle. \tag{7}$$

The projection $F(\tau)$ (that is, the connection between the signal x and Δx in Eq. 1) has here been absorbed into the definition of the apparatus that produces the signal.

Classically, the signal x sees the departure of the length difference between the two arms from the average value. In a static classical space-time with no physical coupling between the two interferometers and no gravitational waves, the average cross correlation vanishes, $\Xi = 0$. However, if the two interferometers share a volume of space-time— that is, if the causal diamonds traced by the propagation of light in their arms overlap in some way— a correlation might be induced by Planckian holographic bounds on the amount of positional information in the system measured by the two sets of optics. They may be entangled by geometrical states in a way that statistically correlates the measurements.

We now propose a simple framework to test the general holographic noise hypothesis: that there is a nonzero correlation between A and B due to entanglement of the emergent space measured by the two interferometers. This framework is formulated in a general way so that the statistical results of a specific experiment can be used to constrain any (future) candidate universal theory of quantum geometry.

Even without a specific fundamental theory, we know that holographic correlations (if they exist at all) are subject to a few simple mathematical and physical constraints.

1. $\Xi(\tau)$ must be symmetric, $\Xi(\tau) = \Xi(-\tau)$. Time symmetry and general covariance dictate that $\Xi(\tau)$ must be either symmetric or antisymmetric. However, Parseval's theorem requires that $\Xi(\tau)$ must have a nonzero value at zero lag if there is to be any measurable fluctuation in a real-valued signal, eliminating the latter choice.

2. The correlation function must respect the causal region in the emergent space. For a simple configuration of two co-aligned Michelson interferometers with characteristic scale L (e.g. arm length), we expect the functional support to be limited by the causal diamond to the interval $\tau = (-L, +L)$ between reflections at the reference world line (e.g. the beamsplitter), or the interval $\tau = (-2L, +2L)$ of events that influence the signal at any given time (see Figure 3). More general interferometer configurations may add additional scales, or even additional world-lines, and yield different functions.

3. The hypothesis being tested is that relative positions of massive bodies as encoded in $\Xi(\tau)$ are subject to Planck scale spreading of information just described. For shear modes (but not rotation), scaling symmetry then requires that where it does not vanish, $\Xi(\tau)$ is linear in τ, with a derivative $d\Xi/d\tau$ that does not depend on the size of the apparatus (see nested causal diamond in Figure 4), but only its shape. To match holographic information content, its absolute value is approximately the Planck time t_P. A more careful evaluation of numerical factors follows below.

With these constraints, for a given apparatus, candidate forms for $\Xi(\tau)$ are completely determined by two parameters. We consider below possible forms for $\Xi(\tau)$ which span the range of consistent options. We also consider how the form of $\Xi(\tau)$ depends on the apparatus configuration— the sizes and relative positioning of two interferometers in space. The detailed worked examples here apply to configurations where the interferometers are adjacent and almost co-located, so that causal diamonds substantially overlap; the simple arrangement reduces the number of parameters needed to characterize the system.

III. PARAMETERIZED MODELS OF CORRELATION FUNCTIONS

A broad class of correlation functions respects the constraints just outlined. The models are described by two parameters that are universal physical constants, that according to the holographic noise hypothesis should not
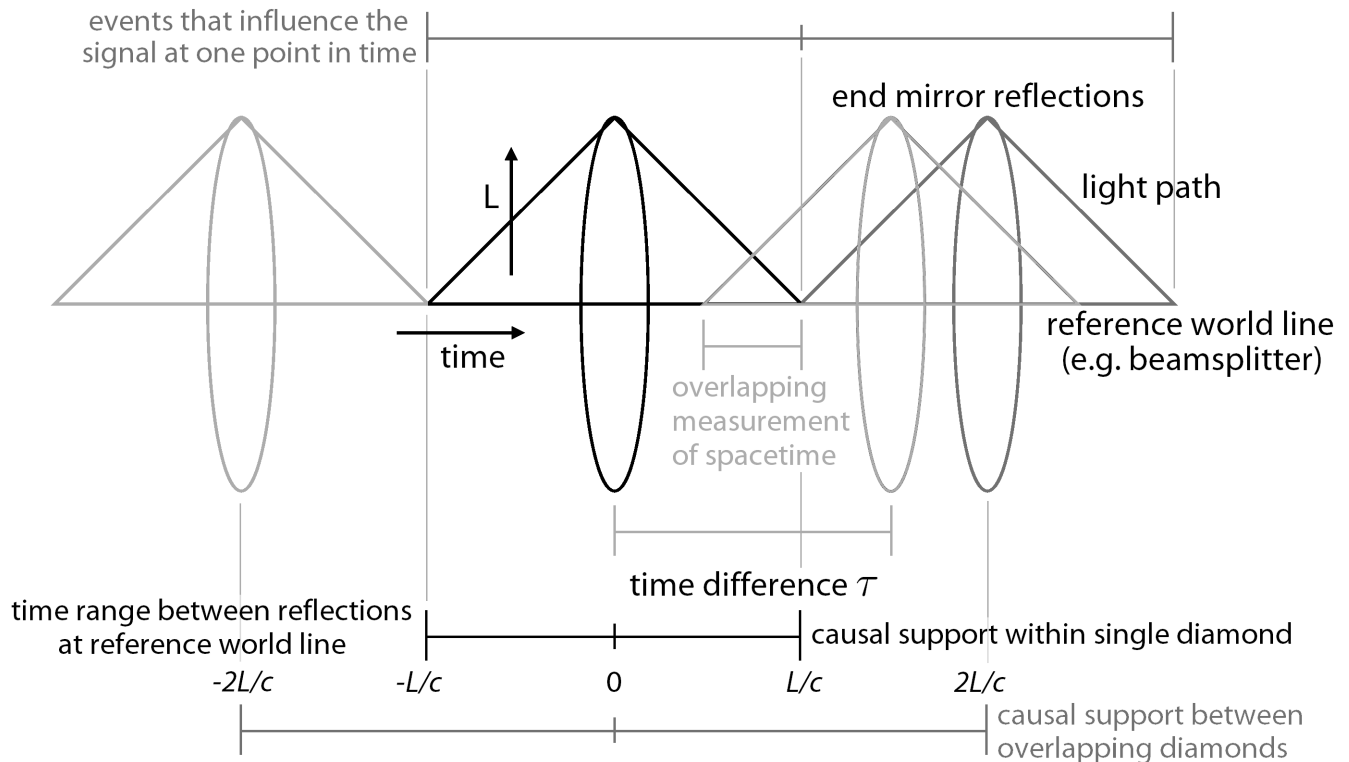
FIG. 3. A comparison of causal support in the two classes of correlation functions.

depend on apparatus size. Two basis vectors, along with upper and lower bounds on normalization, appear to span the space of possibilities consistent with the above constraints.

Following the two viable choices for causal support demonstrated in Figure 3, we first consider a class in which the correlation function goes to zero at the lag corresponding to the edge of the causal diamond defined by the end mirrors. We then present a more general class in which the causal support contains all events that influence the signal at a given time, of which the previous class is a subset.

A.   Simple Case: Models Spanning $\pm L$

In this simplest class of models the correlation is required to drop to zero at $\pm L$, the limits of functional support defined by a single causal diamond. The linearity requirement from scaling symmetry allows us to uniquely specify the correlation function by at most two parameters: the zero lag value normalized to system scale (e.g. arm length),

$$\xi_0 \equiv \Xi(\tau = 0)/L \tag{8}$$

and the norm of the derivative $|\dot{\Xi}|$. In other words,

$$\Xi(\tau) = \begin{cases} \xi_0 L - |\dot{\Xi}| \cdot |\tau| & |\tau| < \frac{L}{c} \\ 0 & |\tau| > \frac{L}{c} \end{cases} \tag{9}$$

According to the holographic noise hypothesis, both ξ_0 and $|\dot{\Xi}|$ are of the order of the Planck time. A choice of ξ_0 and $|\dot{\Xi}|$ predicts a frequency spectrum that can be compared with Holometer data. A set of data can be used to generate a likelihood function for the universal numbers.

The parameter space formed by this class of models is actually one-dimensional, because the derivative is constrained to be (see Figure 4):

$$|\dot{\Xi}| = c\xi_0 \tag{10}$$

reducing the two universal numbers into one parameter that sets the normalization. This simple space is a subset of a more general space of models that allows causal support ranging up to $\pm 2L$, as we will see in the next section.
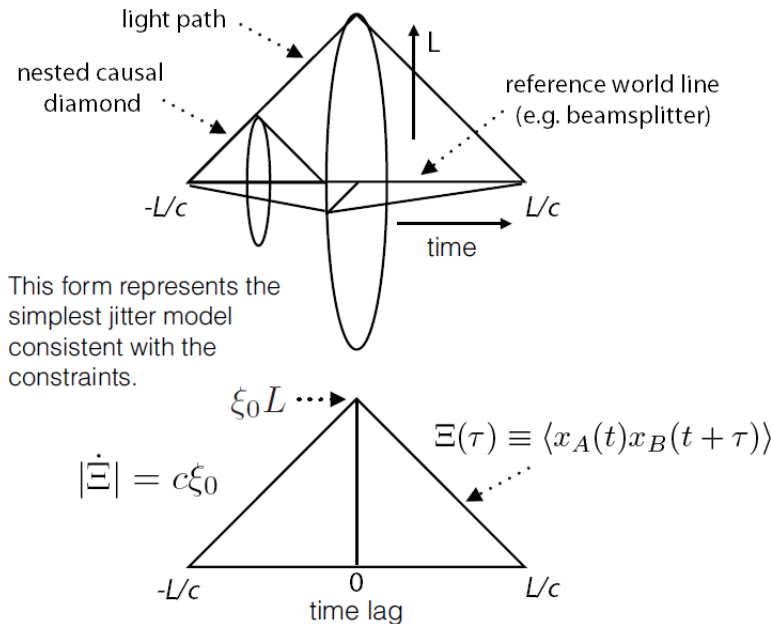
FIG. 4. The simplest model, spanning $\pm L$: Linear time domain cross spectra.

This minimal form of holographic noise can be physically interpreted as a new kind of exotic "jitter" in space and in the position of reference world lines such as the beamsplitter. It was considered as an illustrative model in previous work[30], and used to estimate experimental sensitivity for design purposes.

The fixed value of the derivative might seem overly constraining— the causal diamond support constraint only sets a lower bound on $|\dot{\Xi}|$ at $|\dot{\Xi}| \geq c\xi_0$. We should not discount *a priori* the possibility of steeper slopes, in which case $\Xi(\tau)$ goes negative (with discontinuities at $\pm L$), reflecting more exotic nonlocal correlations in the causal 4-volume. This set of models merely generalizes the simple model of jitter above, and could perhaps be considered physically viable for holographic noise, as long as the integral $\int d\tau\Xi$ remains nonnegative— a condition satisfied by $|\dot{\Xi}| \leq 2c\xi_0$, an upper bound at which there is no DC power in the frequency spectrum because the integral vanishes.

However, a statistical argument eliminates this freedom. For interferometers that are adjacent and almost co-located, the cross-correlation $\Xi(\tau)$ can be thought of as an autocorrelation, since the causal diamonds are almost the same and the geometrical states being measured are substantially entangled. So $\Xi(\tau)$ is an autocorrelation of a real-valued observable, the antisymmetric port beam power (calibrated in length units), undergoing a wide-sense stationary random process. This is possible if and only if the transform $\tilde{\Xi}(f)$ is real, even, and nonnegative at all frequencies [47]. This consideration precludes the viability of models with slopes different from $|\dot{\Xi}| = c\xi_0$.

The analytic form of the frequency domain power spectrum $\tilde{\Xi}(f)$ demonstrates this point:

$$
\begin{aligned}
\tilde{\Xi}(f) &= 2\int_0^{L/c} (\xi_0 L - |\dot{\Xi}|\tau)\cos(2\pi f\tau)\mathrm{d}\tau \\
&= \frac{2|\dot{\Xi}|}{(2\pi f)^2}\left[1 - \cos\left(\frac{f}{c/2\pi L}\right)\right] - \frac{2}{2\pi f}\left(\frac{L}{c}\right)\left(|\dot{\Xi}| - c\xi_0\right)\sin\left(\frac{f}{c/2\pi L}\right) \\
&= \left(\frac{L}{c}\right)^2\left[|\dot{\Xi}|\mathrm{sinc}^2\left(\frac{f}{c/\pi L}\right) - 2\left(|\dot{\Xi}| - c\xi_0\right)\mathrm{sinc}\left(\frac{f}{c/2\pi L}\right)\right]
\end{aligned}
\tag{11}
$$

Normalization from Holographic Gravity

A fundamental theory of emergent geometry should make an exact prediction for the parameters in correlation functions of a given apparatus. In the absence of such a theory, it is useful to have concrete theoretical boundaries where one can reasonably consider a particular hypothesis confirmed or ruled out. We adopt a specific benchmark value as sketched in the appendix. The total number of states within a distance L from holographic or "entropic" gravity is equated with the number of states in a simple noncommutative geometry, a quantum spin system of the same radius. The spin algebra then provides an exact numerical value for the variance of a spatial wave function in

physical length units at separation L:

$$\langle x_\perp^2 \rangle_L / L = \ell_P \equiv ct_P/\sqrt{4\pi} = \sqrt{\hbar G/4\pi c^3} = 4.558 \times 10^{-36}\text{m}. \tag{12}$$

This value sets a benchmark scale of the signal correlation function, $\Xi(\tau = 0)$, that saturates the holographic bound in a causal diamond of radius L. The benchmark scale is to be used for guidance purposes only. The validity of the normalization is independent from the general framework presented throughout the rest of this paper, which relies only on dimensional arguments and first principles of causal consistency and symmetry.

The normalization scheme is valid only for the specific mode of correlation being tested— for the initial stage of the Holometer experiment, these are *shear* modes. The hypothesis being tested is that geometrical information about *directions* between world lines in space obeys Planck scale covariant constraints, which potentially includes shear and rotational modes, but the latter does not follow the same causal structure used for this particular scheme, as will be discussed in upcoming work. The simple Michelson systems considered here are sensitive to strain fluctuations as well as shear ones, but the number of quantum geometric degrees of freedom might scale differently for strain correlations, and the predicted fluctuation amplitudes do not necessarily reach detectable levels when constrained by holographic bounds on information [30, 48, 49]. We consider such strain modes a less viable hypothesis, however, as a coherent and directionally isotropic strain uncertainty likely violates general covariance.

Normalization for Correlated Interferometer Noise

Equation (12) gives a reference scale for the transverse variance associated with distance L, but in order to predict the signal measured in interferometric experiments under this hypothesis, we must conduct a holistic analysis of a quantum-geometrical system of matter and light. It requires a full quantum theory that integrates the Hilbert space of photon states with those of emergent-geometric position states for the mass elements that comprise the optics. In the absence of such a theory, we will establish upper and lower ranges for ξ_0 (and therefore also for $|\dot{\Xi}|$).

A benchmark for ξ_0 is when Eq. (8) and (12) are compared straightforwardly, i.e. $\xi_0 = \ell_P \equiv ct_P/\sqrt{4\pi}$. These describe models that match holographic position uncertainty (and holographic slope, $|\dot{\Xi}| = c\ell_P$).

An upper estimate for ξ_0 is posited when the measurements of two orthogonal arms lengths contribute independent uncorrelated parts to $\Xi(\tau)$. We assume that the transverse variances from Eq. (12) directly apply to the reference world line, as light beams make simultaneous measurements of orthogonal directions at this position.

$$\xi_0 \leq 2\ell_P \equiv ct_P/\sqrt{\pi} \tag{13}$$

Note that we may not count the arm length L twice to account for the round trip time, because doing so while also counting two orthogonal arms would violate quantum limits on information. The holographic bound limits us to the size of the apparatus instead of the whole light path. This normalization is consistent with previous work [30].

The lower bound is saturated when the transverse variance from Eq. (12) is divided between the reference world line (e.g. the beamsplitter) and the end mirror, implying that the equivalent measurable position uncertainty at the reference world line is halved. We also assume that holographic bounds on information limit the measurable noise to the transverse variance from the arm length in one direction, seeing the two orthogonal directions as noncommutative.

$$\xi_0 \geq \frac{1}{2}\ell_P \equiv ct_P/\sqrt{16\pi} \tag{14}$$

We consider this the smallest normalization we can reasonably expect (even under the most conservative assumptions) when all of the holographic uncertainty is manifest in shear mode correlations. If the measured noise is below this level, it likely indicates that at least some of the uncertainty has been squeezed into other unmeasured degrees of freedom such as rotational modes.

The Holometer is expected to reach the sensitivity to detect or rule out all normalizations that are physically plausible.

B. General Class: Models Spanning $\pm 2L$

In this general class of models, the causal support contains all events that influence the signal at a given time, and therefore the correlation does not necessarily drop to zero at the edge of a single causal diamond (representing a single round trip to end mirrors). Instead, we consider the overlap between causal diamonds separated by τ, and maintain functional support for $\Xi(\tau)$ wherever the shared 4-volume is nonzero. We expect $\Xi(\tau)$ to be continuous at the edge
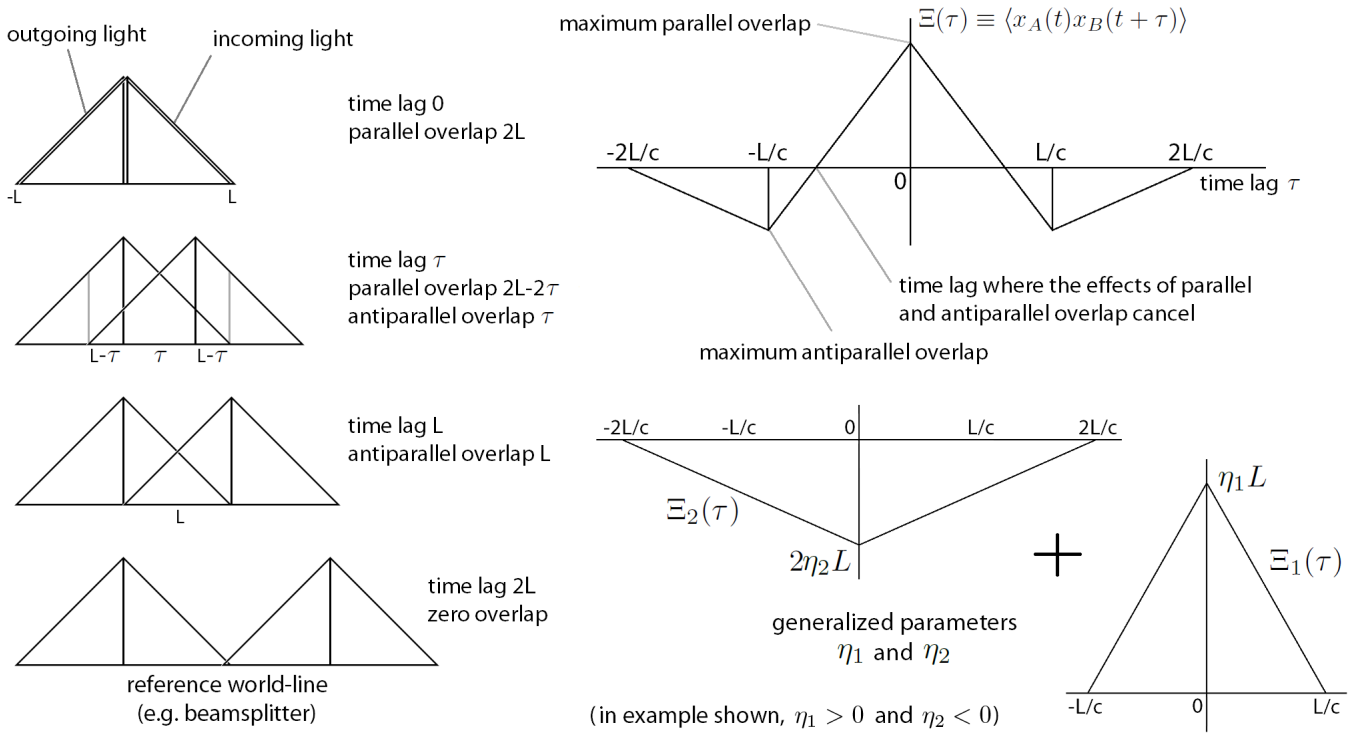
FIG. 5. A generalized class of models, spanning $\pm 2L$: Creating a two-parameter space for all possible correlation spectra. The "baseline model" presented in [30] and tested in [35], a case in which parallel and antiparallel overlaps give equal (positive) contributions, corresponds to a $\pm 2L/c$ triangle with $\eta_1 = 0$, $\eta_2 = +\ell_P \equiv ct_P/\sqrt{4\pi}$.

of a single causal diamond (since the amount of overlap is continuous as a function of τ), and linearly fall off to zero at the edge of the causal limit.

In previous work[30], we presented as an illustrative model a simple triangle spanning $\pm 2L$, physically interpreted as a new kind of exotic "jitter" in space and in reference world line position. This maintains the same form of straightforward linearity used in the previous section, just with longer functional support. In particular, the maximum normalization of this model, corresponding to $\Xi(\tau = 0)/L = 2\ell_P \equiv ct_P/\sqrt{\pi}$, was used as a "baseline model" to estimate experimental sensitivity for design purposes and tested during the initial run of the Holometer[35, 36].

Figure 5 shows the full range of models reflecting a generalized understanding of linearity in this framework of overlapping causal diamonds (and consistent with the constraints outlined in Section II B). The sequence of diagrams on the left hand side shows how the overlap between two causal diamonds changes as the time lag between them increases. In each causal diamond describing an interferometer, the left half represents an outgoing tracer photon propagating towards the end mirrors, and the right half represents an incoming tracer photon coming back towards the reference world line. We use the term "parallel overlap" and "antiparallel overlap" to respectively denote ranges of time where the light path is parallel or antiparallel in direction while the tracer photons in the two interferometers traverse an overlapping 4-volume of spacetime.

An important illustrative case is when the parallel and antiparallel overlaps give contributions to $\Xi(\tau)$ that are opposite in sign (if they are equally weighted, they precisely cancel each other at time lag $\tau = \frac{2}{3}L/c$). The top plot on the right hand side shows an example of $\Xi(\tau)$ under such assumptions. It is naturally a sum of the two plots below it, which define the generalized slope parameters $c\eta_1$ and $c\eta_2$ that establish the parameter space for this class of models. As before, both parameters are on the order of Planck time and not dependent on the apparatus size, and we do not *a priori* constrain them to positive or negative values (despite the illustrative example). A general class of models that contains a linear combination of $\pm L$ and $\pm 2L$ behavior can be written as a parameterized sum,

$$
\begin{aligned}
\Xi(\tau) &= \Xi_1(\tau) + \Xi_2(\tau) \\
&= \begin{cases} \eta_1(L - c\,|\tau|) & |\tau| < \frac{L}{c} \\ 0 & |\tau| > \frac{L}{c} \end{cases} + \begin{cases} \eta_2(2L - c\,|\tau|) & |\tau| < \frac{2L}{c} \\ 0 & |\tau| > \frac{2L}{c} \end{cases}
\end{aligned}
\tag{15}
$$

$$
c\eta_1 \equiv \dot{\Xi}_1(-\frac{L}{c} < \tau < 0) = -\dot{\Xi}_1(0 < \tau < \frac{L}{c}) \quad \text{and} \quad c\eta_2 \equiv \dot{\Xi}_2(-\frac{2L}{c} < \tau < 0) = -\dot{\Xi}_2(0 < \tau < \frac{2L}{c})
\tag{16}
$$

FIG. 6. General parameter space: Two observable length parameters (η_1 and η_2) span all possible models of noise that are consistent with symmetries of spacetime, causal structure, and holographic limits on geometric information. The viable parameter space is defined by two basis vectors (the "$\pm 2L$ triangle" and "zero-DC" models) and and upper and lower ranges on normalization. Sample spectra along the four labeled lines are given in Figure 7.

The two triangle functions, with causal support ranging to $\pm L/c$ and $\pm 2L/c$ respectively, each satisfy the condition for scaling symmetry established in the previous section. We interpret this to mean that we are allowing for two ways in which nonlocal correlations can manifest in the emergent geometry, one that is fully contained within the causal 4-volume of a single diamond (a single round trip to end mirrors) and another that has a causal memory of $\tau = \pm 2L/c$ and depends on the overlap between two causal diamonds.

The former of these effects, reflecting the value of η_1 (or the subspace in which $\eta_2 = 0$), was treated in the previous section on simple models spanning $\pm L/c$. Such cases were discussed in previous work[30] as representing possibilities in which each reflection (when the light interacts with an observer or mass at the end mirror or at the reference world line) sets a boundary condition that resets all quantum geometric information, thereby zeroing the device's response to antiparallel overlap between tracer photon paths before and after an end mirror reflection.

We can now extend this one-dimensional (sub)space into a generalized two-dimensional space defined by universal parameters η_1 and η_2. Similar to the previous class of models, a choice of universal parameter values predicts a frequency spectrum that can be compared with Holometer data. Here, the predictions and data can be used to generate joint likelihood contours.

The constraints on the parameter space derive from similar considerations as before, and the allowed region is plotted in Figure 6. The integral $\int d\tau \Xi$ must be nonnegative, which implies:

$$\eta_1 + 4\eta_2 \geq 0 \tag{17}$$

When the bound is saturated ($\eta_1 + 4\eta_2 = 0$), there is zero DC power in the frequency spectrum, because the integral vanishes. This corresponds to the illustrative case above, where the parallel and antiparallel overlaps give equal-weight
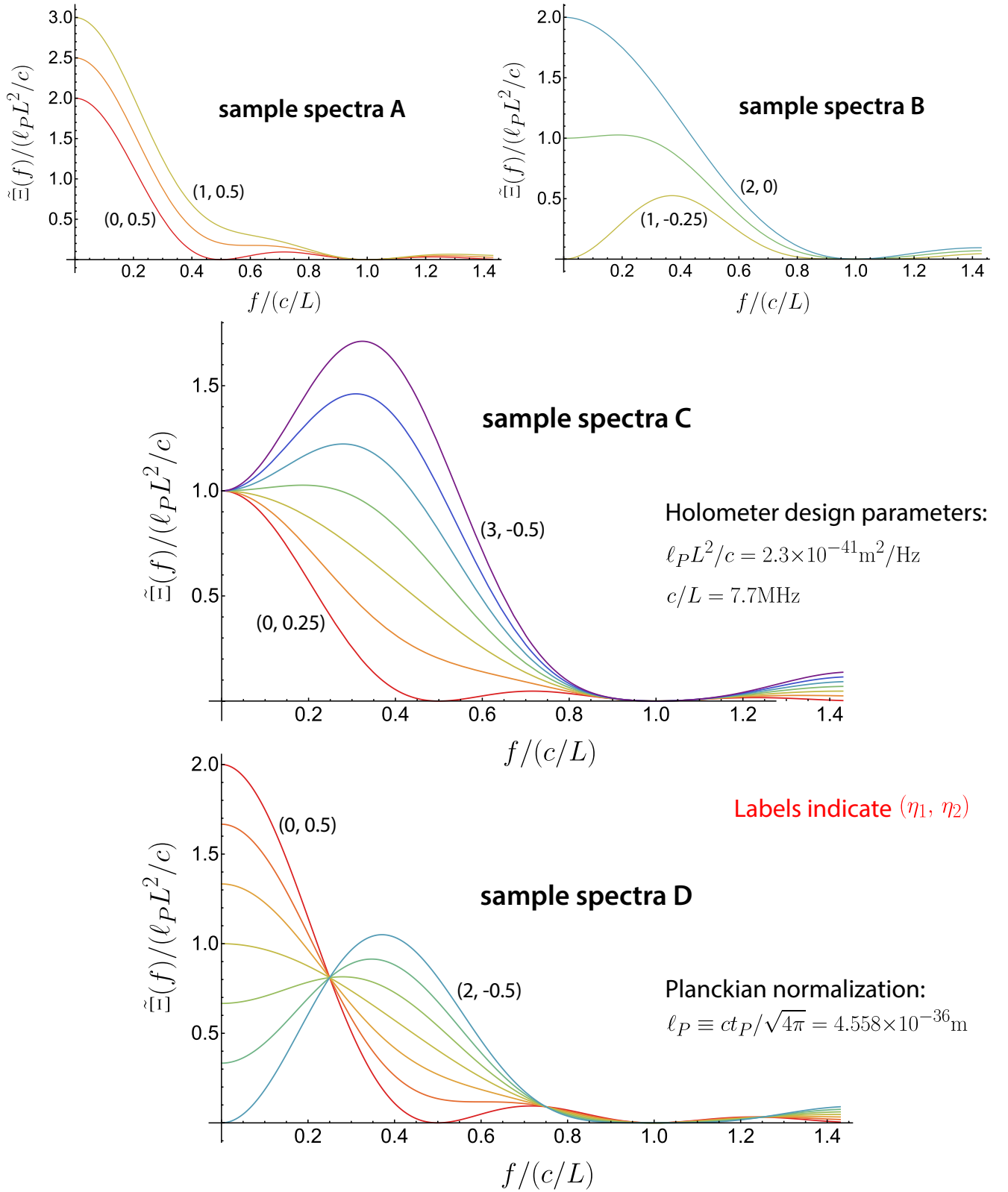
FIG. 7. A representative sample of possible frequency domain spectra. Values of η_1 and η_2 are chosen along the four labeled lines within the parameter space in Figure 6, linearly from left to right, and color-coded along the visible spectrum based on the horizontal location of the model (comparing plots of the same color illustrates differences according to vertical location). Vertical axes are scaled relative to the variance per unit frequency corresponding to $\ell_P \equiv ct_P/\sqrt{4\pi}$ and system scale L. Horizontal axes are scaled to inverse light crossing time for L.
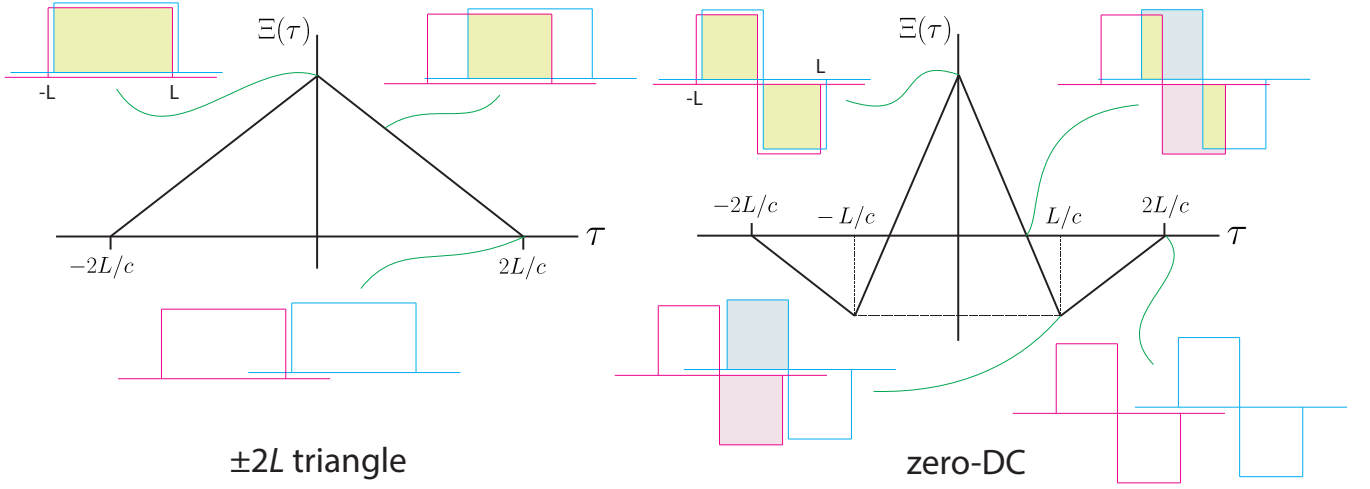
FIG. 8. The basis vectors: The "zero-DC" and "±2L triangle" models, corresponding to flat accumulations of exotic jitter, are generated from autocovariances of ±L boxcar functions that differ by a sign change at the midpoint.

contributions of opposite sign. We physically interpret this as a kind of exotic "jitter" in space (and in world line positions) similar to models considered in previous work[30], but with a different device coupling that flips sign as the light beam reverses direction after an end mirror reflection.

The transform $\tilde{\Xi}(f)$ must be real, even, and nonnegative at all frequencies for $\Xi(\tau)$ to be an autocorrelation of a real-valued wide-sense stationary random process [47]. This requires:

$$\eta_1 \geq 0 \qquad \text{and} \qquad \eta_1 + 4\eta_2 \geq 0 \tag{18}$$

The first part of this constraint makes intuitive sense— we expect stronger positive correlations at time lag under L/c, when there is parallel overlap. When this non-redundant segment of the bound is saturated ($\eta_1 = 0$, $\eta_2 > 0$), the function reduces to the illustrative $\pm 2L$ triangle models considered in previous work, including the "baseline model" [30]. These models get equal positive contributions from parallel and antiparallel overlaps, implying a constant positive device coupling throughout.

The analytic form of the frequency domain power spectrum is helpful for demonstrating these features:

$$\begin{aligned}
\tilde{\Xi}(f) &= 2 \int_0^\infty (\Xi_1(\tau) + \Xi_2(\tau)) \cos(2\pi f \tau) \mathrm{d}\tau \\
&= \frac{2c\eta_1}{(2\pi f)^2}\left[1 - \cos\left(\frac{f}{c/2\pi L}\right)\right] + \frac{2c\eta_2}{(2\pi f)^2}\left[1 - \cos\left(\frac{f}{c/4\pi L}\right)\right] \\
&= c\eta_1\left(\frac{L}{c}\right)^2 \operatorname{sinc}^2\left(\frac{f}{c/\pi L}\right) + c\eta_2\left(\frac{2L}{c}\right)^2 \operatorname{sinc}^2\left(\frac{f}{c/2\pi L}\right)
\end{aligned} \tag{19}$$

Figure 7 shows a sampling of the type of spectra that are expected. The four plots are a representative sample of the mathematical characteristics featured in $\tilde{\Xi}(f)$ as η_1 and η_2 span the range of allowed parameter space.

Basis Vectors for the General Parameter Space

The two bounding cases— the "zero-DC model" ($\eta_1 + 4\eta_2 = 0$, $\eta_1 > 0$, $\eta_2 < 0$) and the "±2L triangle model" ($\eta_1 = 0$, $\eta_2 > 0$)— can be considered basis vectors for this general parameter space. Both correspond to a wide-sense stationary stochastic accumulation of spacetime jitter with constant-magnitude device coupling throughout the light path (or, nonlocally, over measurement time), the only difference being whether the coupling undergoes a sign change halfway through the light storage time (at the end mirror reflection). Figure 8 demonstrates this point. The constant accumulation of fluctuations throughout each round trip is represented by flat boxcar functions of ±L support (with and without the sign change at the midpoint), and the two basis models (both spanning ±2L) are generated from their autocovariances.

These basis vectors can be considered "natural" models where the covariance of exotic correlations follow the causal structure of the spacetime being measured. Here, we use "covariance" in a statistical sense, as opposed to the general

relativistic meaning used throughout the rest of this paper. Adopting the perspective that spacetime is "relational"[1–3], a quantum system woven out of Planckian elements, the spatial structure of their entanglement can be expressed as a statistical covariance among observable operators, with a coherence length and time of the Planck scale. This bottom-up construction from Planckian subsystems, with covariance structures defined by causal surfaces, will be useful in upcoming work as we generalize our predictions to rotational correlations[39, 40].

Normalization for Correlated Interferometer Noise

As with the previous simple class of models (spanning $\pm L$), we will use Eq. (12) and a similar set of assumptions to establish benchmark normalizations and upper and lower ranges for η_1 and η_2 in the general two-parameter space (spanning $\pm 2L$). The viable region of parameter space is plotted in Figure 6.

We first note that, similar to the simpler class,

$$\frac{1}{2}\ell_P \leq \Xi(\tau = 0)/L = \eta_1 + 2\eta_2 \leq 2\ell_P \quad \text{where} \quad \ell_P \equiv ct_P/\sqrt{4\pi}. \tag{20}$$

This, in addition to the constraints from statistical requirements above, automatically sets appropriate ranges for the individual parameters: $0 \leq \eta_1 \leq 4\ell_P$ and $-\ell_P \leq \eta_2 \leq \ell_P$. The upper estimate of $\eta_2 = \ell_P \equiv ct_P/\sqrt{4\pi}$ (with $\eta_1 = 0$) is consistent with the "baseline model" in previous work[30] and was tested during the initial run of the Holometer[35].

As before, as our benchmark normalization matching holographic position uncertainty, we use a straightforward comparison between Eq. (12) and $\Xi(\tau = 0)/L$:

$$\eta_1 + 2\eta_2 = \ell_P \equiv ct_P/\sqrt{4\pi} \,, \qquad |\Xi(\tau)| \leq \ell_P L \tag{21}$$

The Holometer is expected to reach the sensitivity to confirm or reject all physically viable models, exhaustively probing the shear degree of freedom all the way down to our lower bound normalization before leading into the next stage of the experimental program that will test rotational correlations. Quantum geometrical uncertainties can be squeezed into certain degrees of freedom or others due to underlying symmetries in nature or limitations in device coupling; we seek to empirically identify the ones where the information is bounded, guiding the theoretical development.

IV. CURRENT LIMITS AND HOLOMETER SENSITIVITY

The measured spectra at the Holometer are plotted in units of differential arm length (DARM) variance per unit frequency, following the standard conventions adopted by the interferometry community [35, 36]. Since the observables considered in the above predictions for $\Xi(\tau)$ are antisymmetric port signals calibrated to length units, we need to make the following conversion from $\tilde{\Xi}(f)$ to measured power spectral density (PSD):

$$\text{PSD}(f) = \tilde{\Xi}(f) \cdot 2 \cdot \left(\frac{1}{2}\right)^2 = \frac{1}{2}\tilde{\Xi}(f) \tag{22}$$

This is because the dark port signals reflect the optical path difference (OPD) over the full round trip light paths in the two arms. The standard phase-to-length transfer function for Michelson interferometers assumes low-frequency response, in which case OPD $= 2 \cdot$ DARM. Since the measured PSD and $\tilde{\Xi}(f)$ are in units of power (or variance), this factor of $\frac{1}{2}$ gets squared. The remaining additional factor of 2 comes from the fact that $\tilde{\Xi}(f)$ is a standard Fourier transform defined for both positive and negative frequencies, whereas the measured PSD is expressed in the engineering convention, defined only for positive frequencies after folding into the domain the power contained in the redundant negative frequencies.

Figure 9 plots the parameter space constructed above in terms of measured PSD, using universal Planck length units. It demonstrates how this parameter space is used to interpret experimental data and draw constraints on different phenomenological models.

The two lines labeled "GEO-600 noise" reflect upper limits from [50]. Prior to the Fermilab Holometer, GEO-600, employing a single Michelson interferometer with folded arms, was the experiment most sensitive to this type of Planckian geometrical correlation [30]. While it has proven difficult to comprehensively identify and quantify sources of other environmental and technical noise[51], the collaboration has produced a rough upper limit on unidentified flat-spectrum noise (the "signal") around the $1 \sim 6$kHz range where shot noise is dominant and can be reliably modeled, at $1.25 \times 10^{-22}\text{Hz}^{-1/2}$[50] (in strain units). Because this upper limit is only available in a relatively narrow band
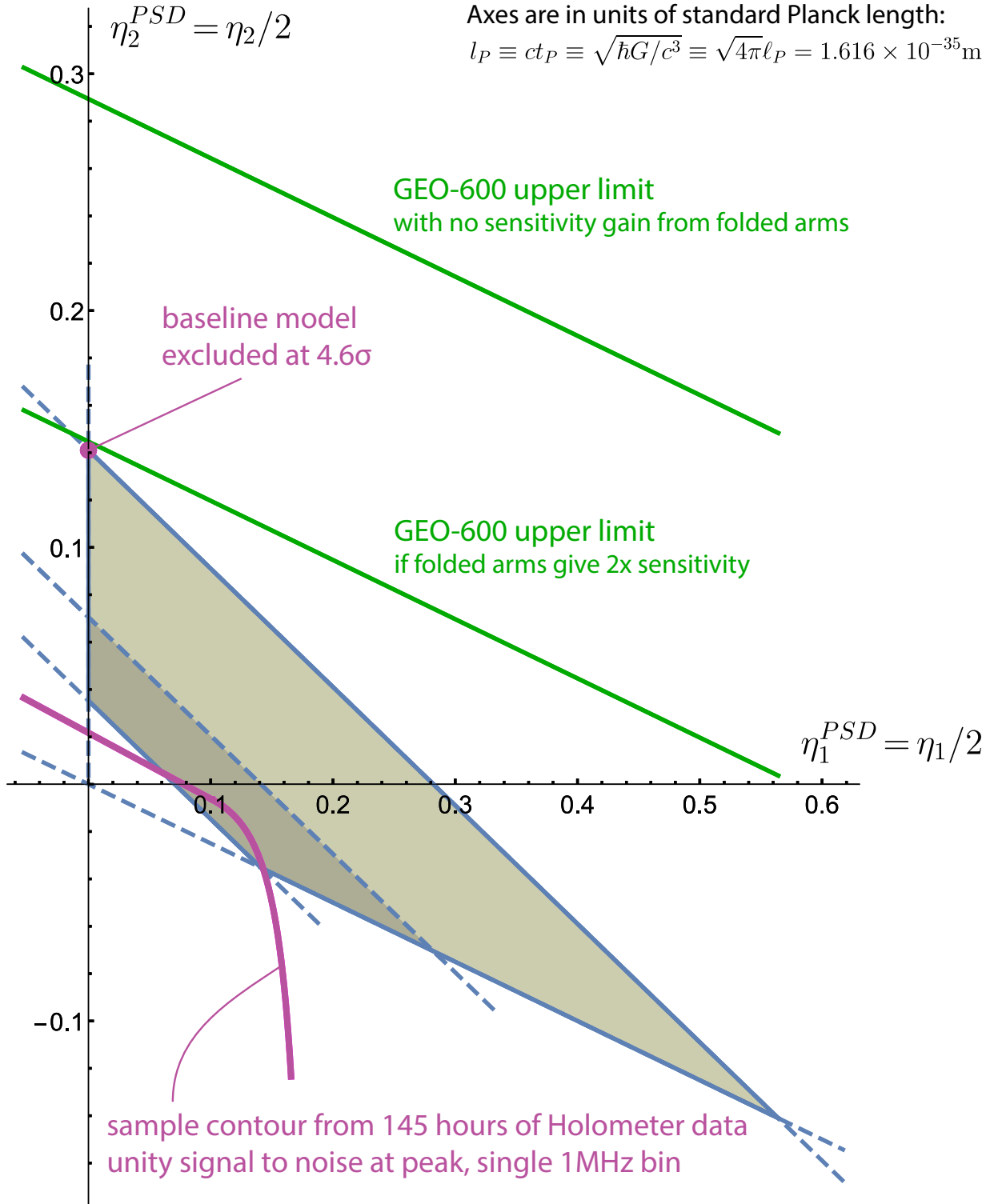
FIG. 9. Current limits and Holometer sensitivity: Upper limits on holographic noise from GEO-600[50] are given under specific assumptions about whether the folded arms lead to a twofold increase in signal power. The illustrative example of "baseline model" from [30] was tested in [35] and ruled out at 4.6σ. Also shown is an example contour of Holometer sensitivity after 145 hours of integration, assuming unity signal-to-noise ratio in a single 1MHz bin at the peak (accurate to $\pm10\%$) [35, 36]. This reflects what we would observe in the case of a null result, as longer integration times are expected to move the contour closer towards zero. If there is a significant detection, the actual likelihood contour would converge around a single point in the parameter space, possibly much farther away from the origin than the plotted example. A highly significant verification or exclusion of the holographic shear noise hypothesis is possible within realistic integration times. Axes are in units of standard Planck length, scaled to power spectral density (PSD) values measurable at the Holometer.

at a frequency much lower than c/L (around 0.5MHz for GEO-600), it can only specify one point on the frequency spectrum and corresponds to a straight line in the parameter space. We plot two lines because it is not clear whether the folded arms in GEO-600 would contribute to a twofold increase in the variance measured in differential arm length. Such considerations were discussed in previous work [30].

The point labeled "baseline model" refers to the illustrative example discussed in previous work[30] and above. It was tested as the nominal model for the initial run of the Holometer. According to the recently released first results, this particular model was excluded at 4.6σ, based on 145 hours of data [35, 36].

For the Holometer, we have also plotted an example contour based on the noise spectrum released with the initial results[35, 36], assuming unity signal-to-noise at the peak of the predicted spectrum corresponding to each point on the contour. Because this sensitivity example is available across a much wider range of frequencies ($1 \sim 6$MHz), we are able to generate contours that cover much wider classes of models that reach maximal power at different frequencies (e.g. Figure 7) instead of a straight line in parameter space like the GEO-600 example.

This is not an exclusion plot, or a likelihood contour at any significance level, and it does not even reflect shot noise-subtracted residual noise like the GEO-600 lines. It is merely intended to demonstrate noise levels attainable at the Holometer, and shows that it takes 145 hours of integration time to get a roughly 1σ result in a 1MHz-wide band at the peak of each modeled spectrum along this contour.

The Holometer operates almost entirely within the frequency range dominated by shot noise. Using the behavior of cross-correlated and integrated shot noise described in [30, 35, 36, 52, 53], it is straightforward to extrapolate the noise levels demonstrated in this example to longer integration times and different choices for frequency binning. An N-fold increase in integration time (or frequency bin width) generally reduces the uncorrelated shot noise power (or error bars in the binned power spectrum) by a factor of $1/\sqrt{N}$, while the correlated exotic Planckian noise remains the same. If we assume that geometry behaves classically up to the level of sensitivity we can project from such extrapolations, a realistic data set would be sufficient to rule out the smallest normalizations within the viable parameter space at roughly 3σ, with the likelihood contour approaching the classical limit at the origin. On the other hand, if a larger signal is detected, the data-based likelihood contour would likely never even reach the example plotted, and instead converge around a specific point within the viable parameter space, with the statistical significance expected to be at least comparable but possibly larger depending on the exact location (a 2000-hour data set would be sufficient for 5σ detection at the edges of the parameter space closest to the origin). The example contour thus demonstrates that the Holometer has the capacity to probe all physically plausible regions within the "shear mode" parameter space, within reasonable integration times.

V.   FUTURE CONFIGURATION: ROTATIONAL MODES

Figure 10 depicts a conceptual big-picture understanding of the overall hypothesis— that geometrical information about directions around world lines is constrained by Planckian bounds defined via general relativistically covariant causal diamonds. In a quantum system of "relational" geometry woven out of causal diamonds containing Planckian subsystems, their spatial entanglement follows statistical covariance structures defined by causal surfaces (note again the two different senses in which "covariance" is used, unlike the general relativistic usage elsewhere in this paper). These null relationships can be decomposed into two orthogonal correlation modes: shear and rotation.

Shear modes couple *transversely* to the arms of a simple Michelson, where light propagates purely radially within the causal diamond. This transverse jitter is manifest as a Planckian spreading of the reference world line, where orthogonal light beams meet at the beamsplitter. The 180° reflections at the end mirrors do not capture the transverse uncertainty, naturally.

Rotational modes[39, 40], on the other hand, cannot be seen in a simple Michelson, because neither the beamsplitter nor the end mirrors have any sensitivity to this type of correlations of quantum-geometrical jitter. To detect them, we add a 90° reflection *away* from the beamsplitter, at significant radial separation, and have a significant portion of the light path involve *angular* propagation. The characteristic scale L for the accumulation of jitter would be the distance between the end mirror and the *bend mirror*, as the latter would be coherent with the reference world line for this type of quantum-geometrical uncertainty. The directional uncertainty, defined in the inertial frame of the reference world line, in this case couples *longitudinally* to the bent portion of the arm. We interpret this as an accumulated effect of the quantum-geometric "twists" of the Planckian elements that comprise the area circumscribed by the bent arm.

In an idealized device, the bent portion of the arm would follow a circular arc, as shown inside a causal diamond in Figure 10. This would ensure a linear form of $\Xi(\tau)$, as the requirements laid out above using the scaling symmetry of causal diamonds would naturally extend here. In fact, if it were possible to have such a device without constant interaction between light and matter, the predicted spectrum would neatly fall into a parameter space spanned by the basis vectors we constructed for the shear case (albeit with different normalizations; see caveats on shear mode
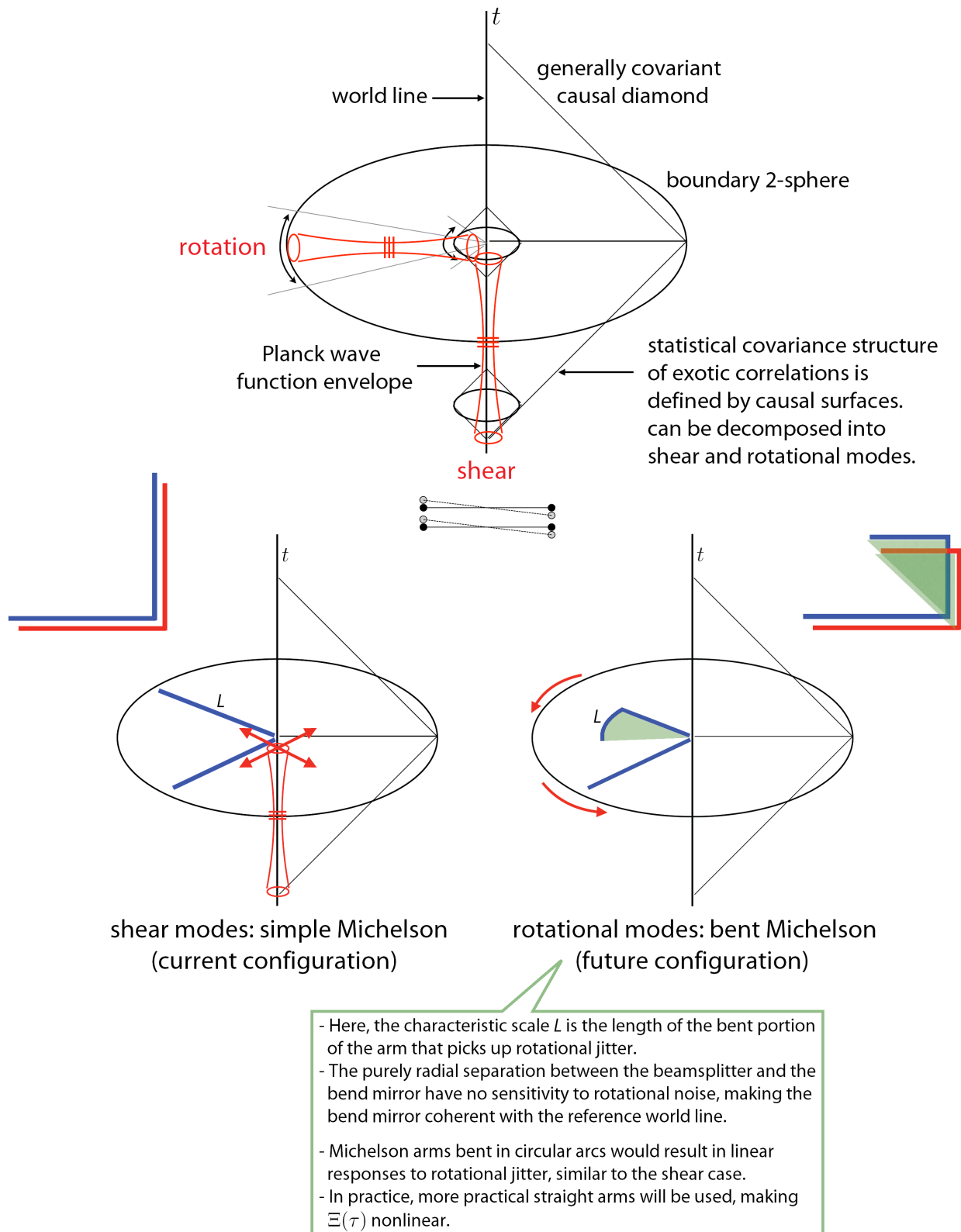
FIG. 10. The statistical covariance structures of exotic Planck-scale geometrical correlations, following null surfaces of causal relations, is shown to decompose into orthogonal modes of shear and rotation. Interferometer setups that couple to each correlation mode are shown: the simple Michelson and bent Michelson setups are capable of detecting shear and rotational noise respectively. Also shown is a spatially extended Sagnac interferometer, optimal for probing Planckian departures from perfect symmetry of inertia.

normalization above). In fact, we expect a response similar to the "zero-DC model," as will be detailed in upcoming work. The precise shape of the predicted spectrum in realistic bent arm configurations (with straight arms) will be calculated in upcoming work.

The Holometer experimental program is designed to complete a comprehensive study of the hypothesized exotic correlations. As seen above, general arguments can set the relevant scaling and amplitude for holographic noise, but not the spatial pattern. There are limited choices for viable spatial patterns: strain, shear, and rotation.

The strain case is not a part of our Planckian *directional* uncertainty hypothesis, as a coherent and directionally isotropic strain uncertainty likely violates general covariance, but it was nevertheless explored with existing data in previous work [30]. Strain noise that scales like $\langle \Delta x^2 \rangle \sim ct_P L$, like we consider here, was ruled out by data from the initial LIGO detectors. Because longitudinal strain noise does not dimensionally reduce the total degrees of freedom, there are arguments for a different scaling behavior $\langle \Delta x^2 \rangle \sim (c^2 t_P^2 L)^{2/3}$ based on a more simplistic interpretation of holographic bounds[30, 48, 49], but those models do not retain coherence, predicting locally observable effects instead of a macroscopic form of nonlocality. These predicted violations of locality have been experimentally ruled out [54–60].

The upcoming results from a long stretch of data under the current simple Michelson design, together with the planned reconfiguration to a bent Michelson setup, should comprehensively probe the two more plausible modes of correlation: shear and rotation. They will either detect specific statistical covariance structures of Planckian correlations in spacetime, or provide concrete evidence for near-perfect Planck scale symmetries of causality and inertia.

ACKNOWLEDGMENTS

---

[1] C. Rovelli. *Quantum Gravity.* Cambridge University Press, 2004.
[2] T. Thiemann. *Modern Canonical Quantum General Relativity.* Cambridge University Press, 2008.
[3] A. Ashtekar. Introduction to Loop Quantum Gravity. *PoS*, QGQGS2011:001, 2011. arXiv:1201.4598 [gr-qc].
[4] S. Deser and P. van Nieuwenhuizen. Nonrenormalizability of the quantized Dirac-Einstein system. *Phys. Rev. D*, 10:411, 1974.
[5] S. Weinberg. *The Quantum Theory of Fields.* Cambridge University Press, 1996.
[6] F. Wilczek. Quantum field theory. *Rev. Mod. Phys.*, 71:S85, 1999.
[7] J. Ellis, N. Mavromatos, and D. V. Nanopoulos. String theory modifies quantum mechanics. *Phys. Lett. B*, 293:37, 1992.
[8] J. Polchinski. *String Theory.* Cambridge University Press, 1998.
[9] S. Hossenfelder. Minimal length scale scenarios for quantum gravity. *Living Rev. Rel.*, 16:2, 2013.
[10] M. R. Douglas and N. A. Nekrasov. Noncommutative field theory. *Rev. Mod. Phys.*, 73:977, 2001.
[11] S. B. Giddings, D. Marolf, and J. B. Hartle. Observables in effective gravity. *Phys. Rev. D*, 74:064018, 2006.
[12] S. B. Giddings. Black holes, information, and locality. *Mod. Phys. Lett. A*, 22:2949, 2007.
[13] T. Banks. Deriving particle physics from quantum gravity: A plan. arXiv:0909.3223 [hep-th], 2009.
[14] T. Banks. Holographic space-time: The takeaway. arXiv:1109.2435 [hep-th], 2011.
[15] J. M. Bardeen, B. Carter, and S. Hawking. The four laws of black hole mechanics. *Commun. Math. Phys.*, 31:161, 1973.
[16] J. D. Bekenstein. Black holes and entropy. *Phys. Rev. D*, 7:2333, 1973.
[17] J. D. Bekenstein. Generalized second law of thermodynamics in black-hole physics. *Phys. Rev. D*, 9:3292, 1974.
[18] S. Hawking. Black hole explosions. *Nature*, 248:30, 1974.
[19] S. Hawking. Particle creation by black holes. *Commun. Math. Phys.*, 43:199, 1975.
[20] G 't Hooft. Dimensional reduction in quantum gravity. In *Conference on Particle and Condensed Matter Physics (Salamfest)*, 1993. arXiv:gr-qc/9310026.
[21] T. Jacobson. Thermodynamics of spacetime: The Einstein equation of state. *Phys. Rev. Lett.*, 75:1260, 1995.
[22] L. Susskind. The world as a hologram. *J. Math. Phys.*, 36:6377, 1995.
[23] R. Bousso. The holographic principle. *Rev. Mod. Phys.*, 74:825, 2002.
[24] E. Verlinde. On the origin of gravity and the laws of Newton. *JHEP*, 1104:029, 2011.

[25] A. G. Cohen, D. B. Kaplan, and A. E. Nelson. Effective field theory, black holes, and the cosmological constant. *Phys. Rev. Lett.*, 82:4971, 1999.

[26] C. J. Hogan. Quantum entanglement of matter and geometry in large systems. arXiv:1412.1807 [gr-qc], 2014.

[27] C. J. Hogan. Measurement of quantum fluctuations in geometry. *Phys. Rev. D*, 77:104031, 2008.

[28] C. J. Hogan. Indeterminacy of holographic quantum geometry. *Phys. Rev. D*, 78:087501, 2008.

[29] C. J. Hogan. Interferometers as probes of Planckian quantum geometry. *Phys. Rev. D*, 85:064007, 2012.

[30] O. Kwon and C. J. Hogan. Interferometric tests of Planckian quantum geometry models. *Class. Quant. Grav.*, 33:105004, 2016.

[31] R. X. Adhikari. Gravitational radiation detection with laser interferometry. *Rev. Mod. Phys.*, 86:121, 2014.

[32] C. J. Hogan. A model of macroscopic geometrical uncertainty. arXiv:1204.5948 [gr-qc], 2012.

[33] C. Affeldt et al. Advanced techniques in GEO 600. *Class. Quant. Grav.*, 31:224002, 2014.

[34] K. L. Dooley for the LIGO Scientific Collaboration. Status of GEO 600. *J. Phys. Conf. Ser.*, 610:012015, 2015.

[35] A. Chou et al. (Fermilab Holometer Collaboration). First measurements of high frequency cross-spectra from a pair of large Michelson interferometers. *Phys. Rev. Lett.*, 117:111102, 2016.

[36] A. Chou et al. (Fermilab Holometer Collaboration). The Holometer: An instrument to probe Planckian quantum geometry. *Class. Quant. Grav.*, 34:065006, 2017.

[37] The LIGO Scientific Collaboration. Advanced LIGO. *Class. Quant. Grav.*, 32:074001, 2015.

[38] The LIGO Scientific Collaboration and The Virgo Collaboration. GW150914: The Advanced LIGO detectors in the era of first discoveries. *Phys. Rev. Lett.*, 116:131103, 2016.

[39] C. J. Hogan. Exotic rotational correlations in quantum geometry. arXiv:1509.07997 [gr-qc], 2015.

[40] C. J. Hogan, O. Kwon, and J. Richardson. Statistical model of exotic rotational correlations in emergent space-time. arXiv:1607.03048 [gr-qc], 2016.

[41] H. Salecker and E. P. Wigner. Quantum limitations of the measurement of space-time distances. *Phys. Rev.*, 109:571, 1958.

[42] C. M. Caves. Quantum-mechanical radiation-pressure fluctuations in an interferometer. *Phys. Rev. Lett.*, 45:75, 1980.

[43] C. M. Caves, K. S. Thorne, R. W. P. Drever, V. D. Sandberg, and M. Zimmermann. On the measurement of a weak classical force coupled to a quantum-mechanical oscillator. I. Issues of principle. *Rev. Mod. Phys.*, 52:341, 1980.

[44] I. Ruo Berchera, I. P. Degiovanni, S. Olivares, and M. Genovese. Quantum light in coupled interferometers for quantum gravity tests. *Phys. Rev. Lett.*, 110:213601, 2013.

[45] A. E. Siegman. *Lasers.* University Science Books, Sausalito, 1986.

[46] C. Gardiner and P. Zoller. *Quantum Noise: A Handbook of Markovian and Non-Markovian Quantum Stochastic Methods with Applications to Quantum Optics.* Springer Series in Synergetics. 2004.

[47] A. V. Oppenheim and G. C. Verghese. *Signals, Systems and Inference.* Pearson Education, 2015. Chapter 11.

[48] Y. J. Ng and H. van Dam. Measuring the foaminess of space-time with gravity-wave interferometers. *Found. Phys.*, 30:795, 2000.

[49] Y. J. Ng. Spacetime foam. *Int. J. Mod. Phys. D*, 11:1585, 2002.

[50] V. Frolov and H. Grote. Gravitational wave detectors in Europe and the U.S. Fermilab Seminar, April 7, 2014. URL: `http://astro.fnal.gov/wp-content/uploads/2014/09/VFrolov_HGrote-040714.pdf`.

[51] S. Hild for the GEO-600 Collaboration. Recent experiments in GEO600 regarding the holographic noise hypothesis. Holographic Noise Workshop, Albert Einstein Institute, May 2009. URL: `http://www.physics.gla.ac.uk/~shild/presentations/holographic_noise_experiments_GEO600.pdf`.

[52] A. Chou, R. Weiss et al. (Fermilab Holometer Collaboration). The Fermilab Holometer: A program to measure Planck scale indeterminacy. 2009. URL: `http://www.fnal.gov/directorate/program_planning/Nov2009PACPublic/holometer-proposal-2009.pdf`.

[53] B. Kamai et al. (Fermilab Holometer Collaboration). The Fermilab Holometer: Probing the Planck scale. In *Am. Astron. Soc. Meeting #221 #431.06*, 2013.

[54] R. Lieu and L. W. Hillman. The phase coherence of light from extragalactic sources: Direct evidence against first-order Planck-scale fluctuations in time and space. *Astrophys. J.*, 585:L77, 2003.

[55] R. Ragazzoni, M. Turatto, and W. Gaessler. The lack of observational evidence for the quantum structure of spacetime at Planck scales. *Astrophys. J.*, 587:L1, 2003.

[56] Y. J. Ng, W. A. Christiansen, and H. van Dam. Probing Planck-scale physics with extragalactic sources? *Astrophys. J.*, 591:L87, 2003.

[57] W. A. Christiansen, Y. J. Ng, and H. van Dam. Probing spacetime foam with extragalactic sources. *Phys. Rev. Lett.*, 96:051301, 2006.

[58] W. A. Christiansen, Y. J. Ng, D. J. E. Floyd, and E. S. Perlman. Limits on spacetime foam. *Phys. Rev. D*, 83:084003, 2011.

[59] E. S. Perlman, Y. J. Ng, D. J. E. Floyd, and W. A. Christiansen. Using observations of distant quasars to constrain quantum gravity. *Astronom. and Astrophys.*, 535:L9, 2011.

[60] E. S. Perlman, S. A. Rappaport, W. A. Christiansen, Y. J. Ng, J. DeVore, and D. Pooley. New constraints on quantum gravity from X-ray and Gamma-ray observations. *Astrophys. J.*, 805:10, 2015.

APPENDIX: NORMALIZATION FROM SPIN ALGEBRA AND HOLOGRAPHIC GRAVITY

It is useful to adopt an exact benchmark value for a Planck scale in absolute physical units, based on the states of a particular quantum system that has both a precisely calculable information content and a precisely calculable position variance. We adopt here the following simple model of a quantum system based on the familiar spin algebra that has these properties, and does not depend on the system dynamics. Of course, just because this model is precise does not mean it is correct. This particular way of counting information[32] is not a necessary assumption for the validity of the generalized framework proposed above, which relies only on first principles such as causal structure and symmetries of spacetime.

Consider a noncommutative geometry described by a standard spin algebra in three dimensions $i, j, k = 1, 2, 3$:

$$[\hat{x}_i, \hat{x}_j] = \hat{x}_k \epsilon_{ijk} i \ell_P. \tag{23}$$

where ϵ_{ijk} denotes the antisymmetric tensor. Consider an operator

$$|\hat{x}|^2 \equiv \hat{x}_i \hat{x}_i, \tag{24}$$

corresponding to the squared modulus of separation, analogous to the square of total angular momentum. Using conventional notation used for angular momentum, let l denote positive integers corresponding to the quantum numbers of radial separation, analogous to total angular momentum. The separation operator takes discrete eigenvalues:

$$|\hat{x}|^2 |l\rangle = l(l+1)\ell_P^2 |l\rangle. \tag{25}$$

We denote the discrete eigenvalues corresponding to classical separation by

$$L \equiv \sqrt{l(l+1)}\ell_P. \tag{26}$$

It can be shown that position $\hat{x}_\perp$ in any direction transverse to separation is indeterminate, with a variance given by

$$\langle \hat{x}_\perp^2 \rangle = L\ell_P. \tag{27}$$

Like spin, the states have a discrete spectrum. The number of position eigenstates within a 3-sphere of radius R can be counted in the same way as discrete angular momentum eigenstates. Using Eq. (26) with $R = L$, the number l_R of radial position eigenstates for a radius R is given by setting $l_R(l_R + 1) = (R/\ell_P)^2$. For each of these, there are $2l + 1$ eigenstates of direction. The total number of quantum position eigenstates in a 3-sphere is then

$$\mathcal{N}_{Q3S}(R) = \sum_{l=1}^{l_R} (2l+1) = l_R(l_R + 2) = (R/\ell_P)^2, \tag{28}$$

where the last equality applies in the large l limit. Thus, the number of quantum-geometrical position eigenstates in a volume scales holographically, as the surface area in Planck units.

We can set an absolute physical scale based on equating the number of states in a 3-sphere from spin geometry and from thermodynamics of gravitational systems[21, 24]. The number of position states for a massive body enclosed in a 3-sphere of radius R that statistically reproduces nonrelativistic Newtonian gravity (cf. [24], Eq. 3.10) is given by:

$$\mathcal{N}_{G3S}(R) = 4\pi (R/ct_P)^2, \tag{29}$$

with the usual definition of Planck length, $ct_P \equiv \sqrt{\hbar G/c^3} = 1.616 \times 10^{-35}$m. Note that this is four times larger than the entropy of a black hole event horizon of the same radius. The quantum-geometrical and gravitational estimates agree, $\mathcal{N}_{Q3S} = \mathcal{N}_{G3S}$, if the numerical value of the effective commutator coefficient ℓ_P is

$$\ell_P = ct_P/\sqrt{4\pi}. \tag{30}$$

If Eq. (30) holds, bodies in the emergent space-time move as described by Verlinde's entropic Newtonian gravity. From Eq. (27), the theory predicts position variance in physical units,

$$\langle \hat{x}_\perp^2 \rangle = Lct_P/\sqrt{4\pi} = (2.135 \times 10^{-18}\text{m})^2 (L/1\text{m}), \tag{31}$$

with no free parameters. A less conservative normalization is to use the holographic principle directly, and equate the number of states in the sphere with those in an event horizon of the same Schwarzschild radius. That gives a larger value, $\ell_P' = ct_P/\sqrt{\pi}$, so it is easier to rule out experimentally.